Journal of
Materials Chemistry B

Materials for biology and medicine

Accepted Manuscript

This article can be cited before page numbers have been issued, to do this please use: C. Ji, Y. Huang, B. Z. Tang and G. Feng, *J. Mater. Chem. B*, 2025, DOI: 10.1039/D5TB01224D.

ROYAL SOCIETY OF CHEMISTRY

rsc.li/materials-b

View Article Online
DOI: 10.1039/D5TB01224D

ARTICLE

Received 00th January 20xx,

Accepted 00th January 20xx

DOI: 10.1039/x0xx00000x

A cationization strategy to simultaneously enhance reactive oxygen species generating and mitochondria targeting ability for enhanced photodynamic therapy

Yankai Huang,[a,#] Chao Ji,[a,#] Ben Zhong Tang,[b] Guangxue Feng[a,*]

Mitochondria-targeted photodynamic therapy (PDT) circumvents the short lifetime and action radius limitation of reactive oxygen species (ROS) and greatly improves the anticancer PDT efficacy. However, current approaches require different molecular engineering strategies to separately improve ROS production and introduce mitochondria targeting ability, which involve tedious synthetic procedures. Herein, we report a facile one-step cationization strategy that simultaneously improve the ROS generation efficiency and introduce mitochondria targeting ability for enhanced PDT. This strategy is demonstrated with AIE-active photosensitizers ITPAPy, where cationization transforms the pyridine ring in ITPAPy into a positively charged pyridinium salt in ITPAPyI. Cationizaiton promotes intramolecular charge separation and enhances intersystem crossing without compromising the AIE properties, and ITPAPyI generates higher levels of ROS over its neutral counterpart ITPAPy. Moreover, the cationic ITPAPyI profoundly enriched at mitochondrial membrane of cancer cells, while the neutral ITPAPy mainly accumulated in lysosomes. Since mitochondria are the main target of ROS, ITPAPyI causes massive oxidative damage to mitochondria and promote apoptosis, showing a more effective PDT effect. This cationic molecular engineering strategy establishes an attractive paradigm for designing photosensitizers with concurrent ROS enhancement and mitochondria-targeting capabilities, paving the way for highly efficient PDT applications.

1. Introduction

Cancer poses a serious threat to global public health, with increasing morbidity and mortality worldwide in recent years.[1] Compared with conventional cancer treatment approaches such as surgery, chemotherapy and radiotherapy, photodynamic therapy (PDT) offers superior spatiotemporal precision and minimal invasiveness, enabling selective tumor ablation while sparing normal tissues from damage.[2-3] PDT relies on light excitation of photosensitizers (PSs) to generate toxic reactive oxygen species (ROS) to cause cell component oxidation and damage.[4-6]Upon light activation, photosensitizers will be excited from the ground state (S_0) to the singlet excited state (S_1), and further undergo intersystem crossing (ISC) to reach the long-lived triplet excited state (T_1). These T_1-stated photosensitizers could further react with surrounding oxygen to generate ROS, in particularly singlet oxygen ($^1O_2$), that cause cancer cell death.[7-10] However, most conventional photosensitizers (e.g., porphyrin, BODIPY, PDI) possess planar π-conjugated structures that tend to aggregate in aqueous microenvironments, tumor tissues or enriched areas, leading to π-π stacking and reduced ROS generation – a phenomenon known as aggregation-caused quenching (ACQ).[11-13] This notorious ACQ effect greatly hinders the therapeutic efficacy of PDT. In addition, the extremely short lifetime and limited diffusion radius of ROS in biological systems through minimize the off-target damage to normal tissues,[15-17] it also leads to an unsatisfactory cancer-killing effect when photosensitizers are located away from their targets.[18,19] Therefore, it is highly important to develop photosensitizers with high ROS generation and close proximity to intracellular targets to achieve effective PDT damage.[20]

Aggregation-induced emission (AIE) photosensitizers have emerged as a promising alternative, which ideally overcome ACQ effect and enhance ROS generation under physiological conditions.[21-24] These AIE fluorogens (AIEgens) usually have negligible fluorescence in the molecular state but show largely enhanced emission in the aggregated state due to the restriction of the intramolecular motion (RIM) that suppresses the non-radiative pathway.[25-27] The suppression of non-radiative dissipation also promotes ISC process for better ROS generation.[24,28] Owing to these properties, AIEgens have been utilized to develop light-up probes, activatable photosensitizers, effective nano-photosensitizers, etc. To further improve the PDT efficacy and circumvent the lifetime and diffusion radius limitations of ROS, AIE photosensitizers that target subcellular organelles such as the membrane,

[a] *State Key Laboratory of Luminescent Materials and Devices, Guangdong Provincial Key Laboratory of Luminescence from Molecular Aggregates, School of Materials Science and Engineering, South China University of Technology, Guangzhou, 510640, China*
[b] *Shenzhen Institute of Aggregate Science and Engineering, School of Science and Engineering, The Chinese University of Hong Kong, Shenzhen 518172, China*
[#] These authors contributed equally to this work.
* Corresponding authors: fenggx@scut.edu.cn
Supplementary Information available: [details of any supplementary information available should be included here]. See DOI: 10.1039/x0xx00000x

View Article Online
DOI: 10.1039/D5TB01224D

endoplasmic reticulum (ER), lysosome, etc., have beendeveloped.[29-33]In particular,

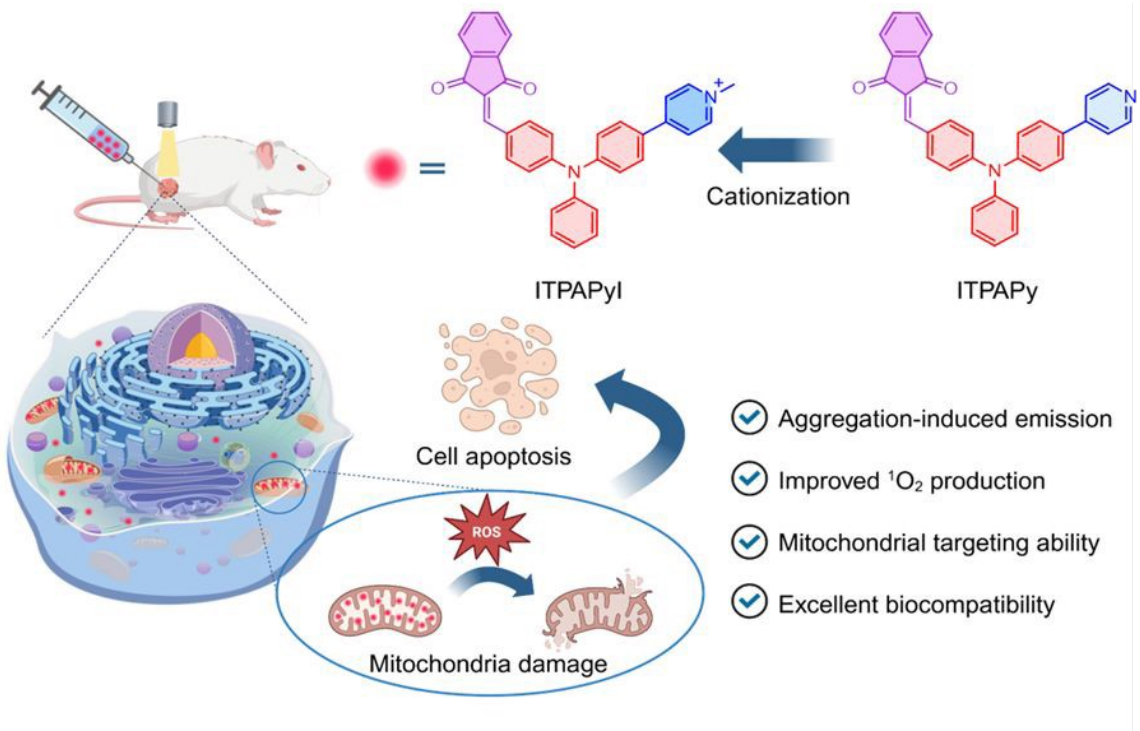

Scheme 1. Schematic of the cationization of ITPAPy into ITPAPyI to improve its ROS generation and mitochondria targeting ability for enhanced PDT.

mitochondria are the powerhouses of cancer cells that promote cancer metastasis, and their dysfunction also plays a central role in mediating apoptosis. Therefore, mitochondria have been recognized as a new pharmacological target for cancer therapy and the primary target of PDT.[34-37]

By localizing photosensitizers to mitochondria, the directly generated ROS could depolarize mitochondrial membrane potential, cause oxidative stress, and greatly trigger programmed cell death pathways, such as apoptosis and pyroptosis.[37-39] Additionally, ROS may also damage the electron transport chain complex on the inner mitochondrial membrane and block ATP generation, disrupting the energy metabolism and inhibiting cancer proliferation.[40-42] Various mitochondria-targeting photosensitizers have been developed by introducing triphenylphosphine, quaternary ammonium, and other mitochondria-targeting groups to photosensitizers.[43,44] However, these targeting moieties are usually linked to photosensitizers via alkyne chains, and their presence minimally affects the ROS generation ability. It often requires different molecular engineering strategies to separately improve ROS production and introduce mitochondria targeting ability, which involves tedious chemical synthetic procedures.[43,45] In this regard, a more facile molecular design approach that could simultaneously enhance ROS generation and mitochondria targeting is urgently needed for effective PDT.

In this work, a cationization strategy is reported to simultaneously enhance ROS generation and enable mitochondrial targeting to develop mitochondria-targeted AIE photosensitizers for enhanced PDT (Scheme 1). An AIE-active molecule, ITPAPy was firstly developed as the precursor, which features triphenylamine as the central electron donor, indanedione and pyridine as acceptors. Benefiting from its AIE-active structure, ITPAPy exhibited a typical AIE effect and efficient ROS generation in the aggregated state. In addition, quaternizating the pyridine unit of ITPAPy yielded the cationic AIE photosensitizer ITPAPyI. This cationization enhances the electron-withdrawing capability of the pyridine ring, which promotes intramolecular charge separation and enhances ISC without compromising the AIE properties.[46, 47] As a result, the cationic AIE ITPAPyI generates higher levels of ROS, particularly singlet oxygen over its neutral counterpart ITPAPy. More importantly, the positive charge also facilitates the accumulation of ITPAPyI to the negatively charged mitochondrial membrane of cancer cells, while the neutral ITPAPy mainly accumulated in lysosomes. Since mitochondria are the main target of ROS, their close proximity could cause oxidative damage to mitochondria and promote apoptosis, leading to a more effective PDT effect. Therefore, this cationic molecular engineering strategy can provide an attractive paradigm for photosensitizer design with concurrent ROS enhancing and mitochondria targeting capability for effective PDT.

2. Results and Discussion

2.1 Synthesis and characterization of AIE photosensitizers

View Article Online DOI: 10.1039/D5TB01224D

In our molecular design, triphenylamine (TPA) with twisted geometry was selected as the electron donor, which helps to realize the AIE effect and promote ROS generation in the aggregated state. In addition, indanedione (IN) and pyridine (Py) were selected as peripheral electron acceptors to promote intramolecular charge transfer (ICT) effect. Py cationization should improve the spatial separation of the the highest occupied molecular orbital (HOMO) and the lowest unoccupied molecular orbital (LUMO), facilitating ISC process. [48]Further density functional theory (DFT) calculations (B3LYP/6-31G (d, p)) showed that HOMO was mainly located in the central TPA part for both molecules, while LUMO shifted from the IN segment (for ITPAPy) to PyI segment (for ITPAPyI) with a larger HOMO-LUMO separation (Figure S12). This suggests the more efficient intersystem crossing process and better ROS generation for cationic ITPAPyI.[49, 50] The detailed synthetic routes towards ITPAPy and ITPAPyI are shown in Figure S1 and their chemical structures were confirmed by ^{1}H and ^{13}C NMR spectrometry, and high-resolution masspectrometry (HR-MS) (Figures S2-S11).

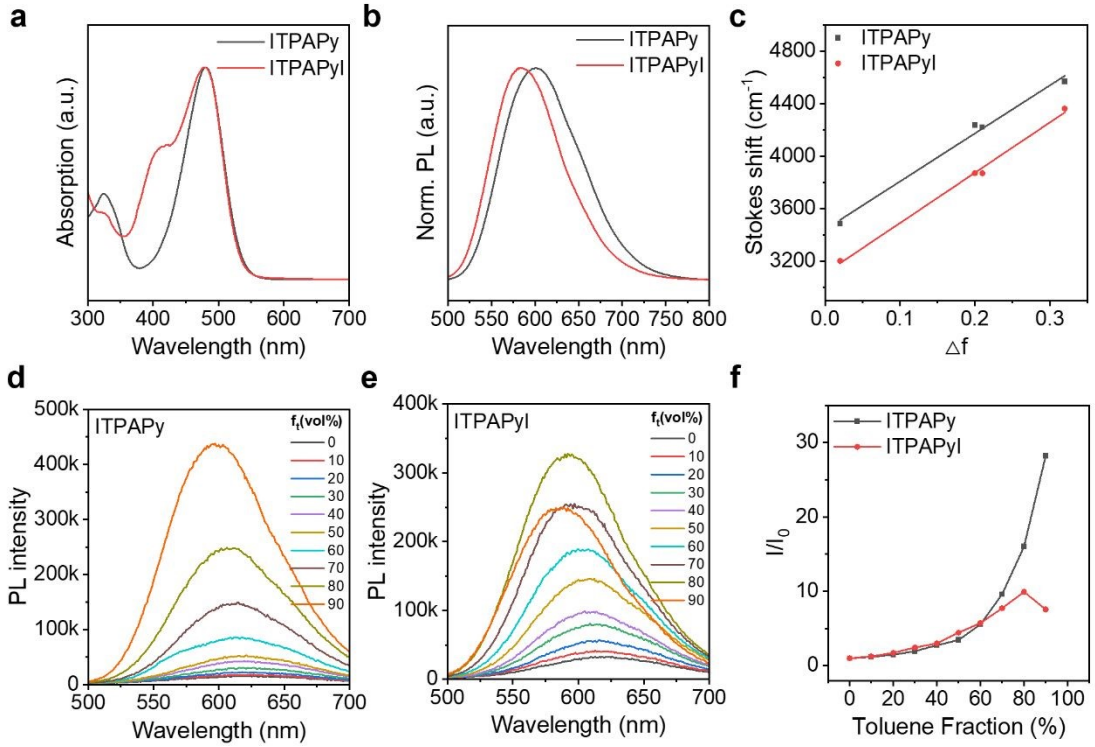

Figure 1. (a) Normalized absorption spectra of ITPAPy and ITPAPyI in DMSO. (b) Normalized PL spectra of ITPAPy and ITPAPyI in DMSO. (c) Plots of the Stokes shifts of ITPAPy and ITPAPyI vs the orientation polarizability (△f). (d) PL spectra of ITPAPy in DMSO/toluene mixtures with different toluene fractions (f_t). (e) PL spectra of ITPAPyI in the mixture of DMSO/toluene mixtures with different f_t. (f) Plot of relative PL intensity (I/I_0) vs f_t in the DMSO/toluene, I_0 is the PL intensity of AIE PSs in pure DMSO, and I is the PL intensity of AIE PSs in the mixture. ([AIE PSs] = 5 μM).

The photophysical properties were first investigated by UV-vis and photoluminescence (PL) spectroscopies. The absorption and emission spectra of ITPAPy and ITPAPyI were tested in DMSO. Their maximum absorption and emission peaks are located at 488 nm and 600 nm, respectively, with ITPAPyI showing an absorption shoulder around 400 nm, which is beneficial for harvesting the whole spectrum energy of white light (Figure 1a,1b). To study the ICT effect, their absorption and emission spectra were measured in solvents of different polarities. Both absorption and emission maxima of ITPAPy and ITPAPyI red-shifted with the increase of solvent polarities. In addition, ITPAPyI exhibited an emission peak red-shift of 67 nm when changing the solvent from toluene to DMSO, which is slightly larger than that of ITPAPy (65 nm) (Figure S13). Lippert-Mataga plot was further performed to further quantify their ICT degree (Figure 1c). With the increased solvent-oriented polarizability (Δf), ITPAPyI showed a slightly larger Stokes shift, with a slope (Stokes' shift versus polarizability) of 3827.85, which is slightly larger than that of ITPAPy (3661.49), hinting the stronger ICT effect of ITPAPyI.[51] In addition, the AIE features of ITPAPy and ITPAPyI were evaluated with DMSO as the good solvent and toluene as the poor solvent (Figure 1d,1e). Upon addition of toluene into the DMSO solution to induce the aggregate formation, the fluorescence intensities of both ITPAPy and ITPAPyI effectively enhanced with the increased toluene fractions (f_t). The α_{AIE} values (the ratio of the highest fluorescence intensity in toluene/DMSO mixture to that in DMSO) were determined to be 28.22 and 9.33 for ITPAPy and ITPAPyI, respectively, indicating their AIE characteristics (Figure 1f).

2.2 ROS generation of AIE photosensitizers

View Article Online DOI: 10.1039/D5TB01394D

The ROS-generating ability of these AIE photosensitizers was further tested. Non-emissive dichlorodihydrofluorescein (DCFH), which can be converted to green fluorescent dichlorofluorescein DCF upon irreversible reaction with ROS, was used as an overall ROS indicator. The commercial photosensitizer Rose Bengal (RB) was selected as the benchmark. Under white light irradiation (20 mWcm^{-2}), all these three photosensitizers readily intensified the green fluorescence of DCF within 60 s (Figure 2a-2c). Specifically, ITPAPy led to a DCFH fluorescence enhancement factor of ~38.4, similar to that induced by RB (~35.1), indicating their similar ROS generation ability. In contrast, ITPAPyI showed a DCFH enhancement factor of 47.6, which was about 1.24-fold higher than ITPAPy, suggesting that the cationization could enhance ROS generation. 9,10-Anthracenediyl-bis(methylene)dimalonic acid (ABDA) was further used to test the generation of $^1O_2$, which is the primary ROS that delivers therapeutic effect in PDT applications (Figure 2d,2e).[52] ABDA itself showed minimal absorbance decreased after white light irradiation of 60 s. However, ITPAPyI decreases the ABDA absorbance to 60.9% of the initial value under the same conditions, indicating that ITPAPyI could effectively generate $^1O_2$ under light conditions (Figure 2f). On the other hand, both RB and ITPAPy exhibited similar and slower ABDA decomposition rate, suggesting their similar $^1O_2$ generation ability, in consistence with the DCF results (Figure S14). In addition, $^1O_2$ quantum yields of ITPAPy and ITPAPyI were calculated to be 84.0% and 9.9%, respectively with RB (76%) as the benchmark. Additionaly, electron paramagnetic resonance (ESR) analysis, with 5,5-dimethyl-1pyrroline N-oxide (DMPO) and 2,2,6,6-tetramethyl-1-piperidine (TEMP) as trapping agents, further showed that only ITPAPyI produces $^1O_2$ while both molecules moderately generate radical type ROS (Figure S15). Collectively, our results suggested that the cationization could enhance the ROS, especially $^1O_2$ generation ability.

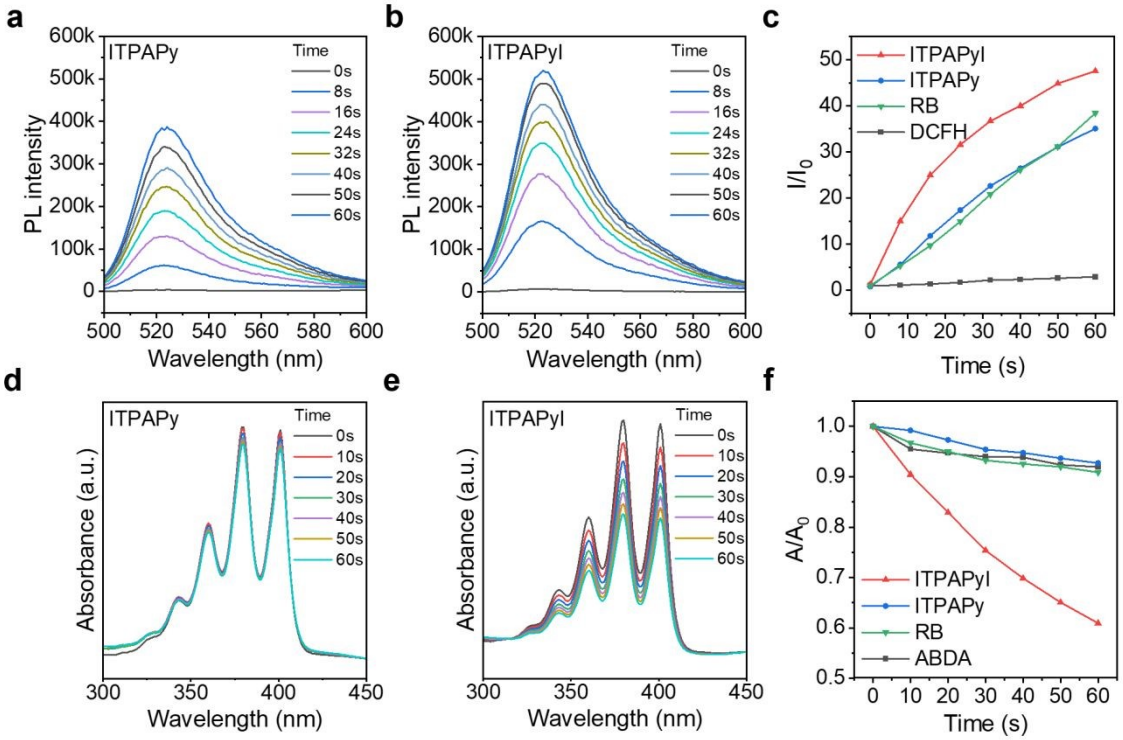

Figure 2. PL spectra of DCFH in the presence of (a) ITPAPy and (b) ITPAPyI upon light irradiation. (c) DCFH fluorescence enhancements in the presence of different photosensitizers. Absorption spectra of ABDA in the presence of (d) ITPAPy and (e) ITPAPyI upon light irradiation. (f) ABDA decomposition profiles in the presence of different photosensitizes. [AIE PSs] = 10 μM, [DCFH] = 50 μM, [ABDA] = 50 μM.

2.3 Intracellular localization of AIE photosensitizers

The cellular uptake and intracellular location of both AIE photosensitizers were subsequently evaluated. MCF-7 breast cancer cells were incubated with ITPAPy and ITPAPyI (5 μM) for 2, 4, 6, 8, and 12 h, respectively. With the increase of incubation time, bright red fluorescence started to emerge and increase inside MCF-7 cells (Figure 3a). The intracellular fluorescence reached the plateau at 8 h of incubation, suggesting their effective cellular uptake. ITPAPyI also showed a better cellular uptake to MCF-7 cancer cells over L929 normal cells, attributing to the more negative surface charge of cancer cells (Figure S16). In addition, very distinct fluorescence patterns were observed for ITPAPy and ITPAPyI. ITPAPy treated cells showed dot-like fluorescence enriched at a specific location, while ITPAPyI-treated cells showed network-like fluorescence. This suggests that ITPAPy potentially accumulates at lysosome, while ITPAPyI likely targets mitochondria. To confirm their intracellular localization, these cells were further co-stained with LysoTracker Green FM and Mito Tracker Green FM. As shown in Figure 3b and 3c, the red fluorescence of ITPAPy overlaps very well with LysoTracker Green FM, with a Pearson correlation

coefficient of 0.97, while ITPAPyI overlaps well with Mito Tracker Green FM with a Pearson correlation coefficient of 0.92, respectively. In addition, a linear region of interest (ROI) line was also drawn on these CLSM to confirm their co-localization. As shown in Figure 3b, the fluorescence intensity curves of AIE photosensitizers well overlapped with those of LysoTracker or MitoTracker, suggesting the excellent lysosomal targeting ability of ITPAPy and mitochondrial targeting ability of ITPAPyI, respectively. The distinct subcellular organelle targeting ability shall be due to the presence of the neutral and positive formats of the pyridine ring. The presence of nitrogen atoms endows ITPAPy with a certain basicity, increasing its affinity towards hydrogen ions, which are usually enriched in the acidic lysosomes (with an internal pH value of 4.5-5.0), and thus ITPAPy specially accumulated at lysosomal sites.[53-55] On the other hand, ITPAPyI with the positive charge could specially target the negatively charged mitochondria inner membrane.[56] In addition, the intracellular localization of both ITPAPy and ITPAPyI was not affected by the acidic microenviroments (Figure S17). Therefore, the cationic pyridine group not only enhances the ROS generation but also brings ITPAPyI close to its main target mitochondria, which is expected to exhibit largely enhanced PDT performance.

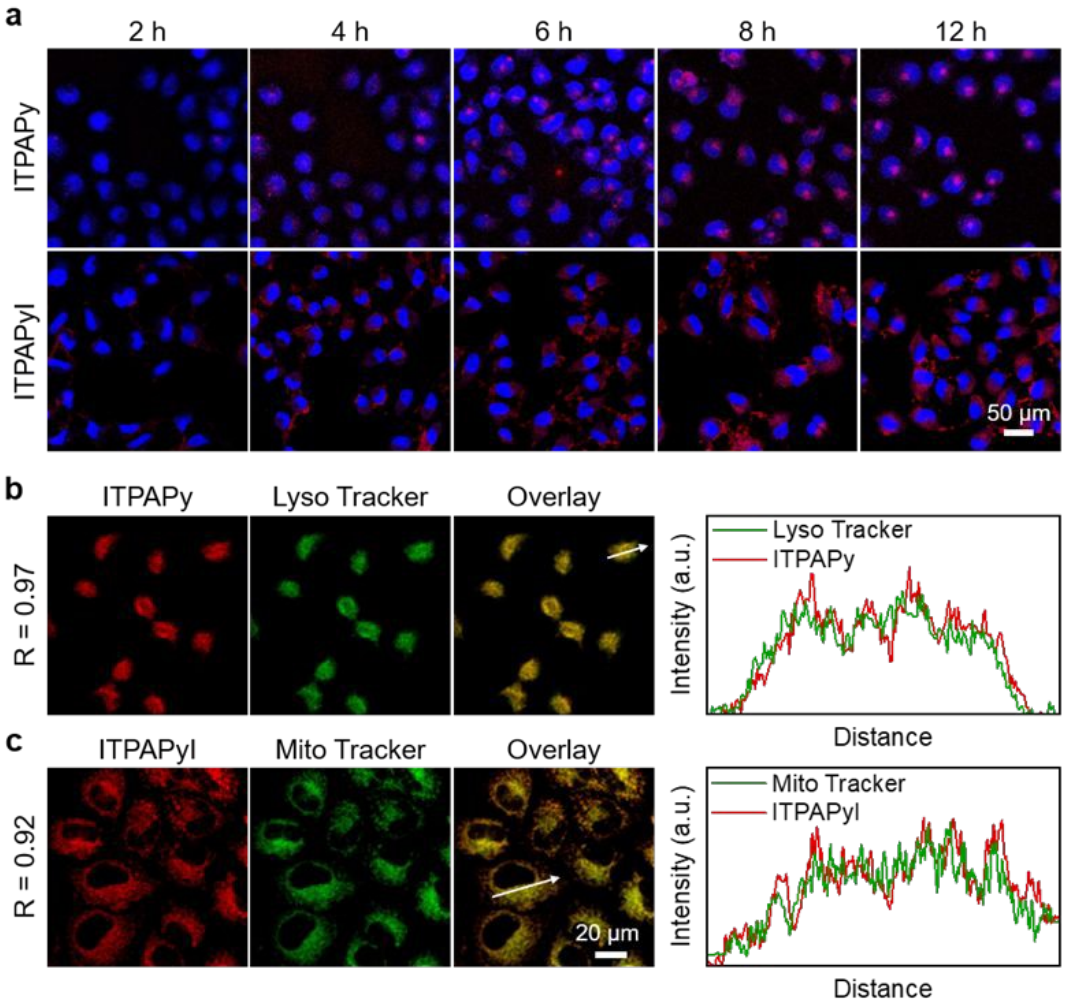

Figure 3. (a) CLSM images of MCF-7 cells incubated with ITPAPy and ITPAPyI for different time followed by staining with Hoechst 33342. (b) CLSM images of MCF-7 cells incubated with ITPAPy followed by co-staining with LysoTracker Green FM, and the intensity profile of the linear region of interest (ROI) across the cell. (c) CLSM images of MCF-7 cells incubated with ITPAPyI followed by co-staining with MitoTracker Green FM, and the intensity profile of linear ROI across the cell. [AIE PSs] = 5 μM, [Hoechst 33342] =1 μgmL^{-1}, [LysoTracker Green FM] = 500 nM, [MitoTracker Green FM] = 500 nM.

2.4 *In vitro* PDT of AIE photosensitizers

The ability of ITPAPy and ITPAPyI to generate ROS intracellularly was then investigated. Both AIE photosensitizers were incubated with MCF-7 cells for 8 h, followed by 2',7'-dichlorodihydrofluorescein diacetate (DCFH-DA) staining, and light irradiation. As expected, cells from both ITPAPy + L (L refers to light irradiation) and ITPAPyI + L group showed significantly intensified green fluorescence signals, while these from the control and dark groups emitted minimally (Figure 4a). ITPAPyI + L group exhibited an intracellular green fluorescence that was 1.92-fold higher than the ITPAPy + L group (Figure S18), confirming the better intracellular ROS generation of ITPAPyI. The cancer cell ablation ability of both AIE photosensitizers was further visualized by a live/dead staining assay with calcein

AM/propidium iodide (PI) assay. Control and dark groups showed only green fluorescence emitted by calreticulin AM, indicating that cancer cells maintained good viability when no ROS were produced inside cancer cells (Figure 4b). After light irradiation, red fluorescent cells started to emerge at the expense of green live cells, suggesting that light-simulated ROS killed cancer cells. In addition, the co-existence of both green and red fluorescence was observed in the ITPAPy + L group, while the dominance of red fluorescence in the ITPAPyI + L group clearly proved the better cancer cell killing effect of the cationic AIE photosensitizer ITPAPyI (Figure S19).

To access the oxidative damages to mitochondria, Rhodamine 123 (Rho123), a lipophilic cationic fluorescent dye that detects the mitochondrial transmembrane potential (ΔΨm), was employed. Rho123 enriches in the healthy mitochondrial matrix through an electrochemical gradient. However, Rho123 will be released from mitochondria when the mitochondria membrane potential decreases, resulting in a markedly reduced yellow-green fluorescence in mitochondria. As shown in Figure 4c, intense green fluorescence of Rho123 in dark groups and PBS + L group indicated the intact mitochondria membrane potential. Similar strong Rho123 fluorescence was also observed in the ITPAPy + L group, suggesting that the generation of ROS in lysosome caused minimal oxidative damage to the cancer cell mitochondria. In contrast, markedly reduced fluorescence and diminished mitochondria network were observed in ITPAPyI + L groups, indicating the dysfunction of mitochondria. Semiquantitative analysis further showed that the mitochondria fluorescence of Rho123 in ITPAPyI + L group was only 43.4% of ITPAPy + L group, 34.5% of PBS group (Figure S20), confirming that the close proximity of photosensitizers and mitochondria could greatly cause mitochondrial damage.

The cell viabilities were further quantitatively assessed by the standard 3-(4,5-dimethylthiazol-2-yl)-2,5-diphenyltetrazolium bromide (MTT) assay. ITPAPy and ITPAPyI themselves in dark exhibited minimal toxicity to cancer cells, where the survival rate of MCF-7 still remained almost 100% at high concentrations (Figure 4d). However, light-irradiating photosensitizer-treated cells caused a sharp decrease in cell viability. For instance, at an incubation concentration of 16 μM, the cell survival rate in the ITPAPy + L group was 67.28%, which was reduced to 21.18% in the ITPAPyI + L group. The half-maximum inhibition concentration (IC_{50}) was further determined to be 26.91 and 7.08 μM for ITPAPy and ITPAPyI under light irradiation. The better cancer cell killing ability of ITPAPyI shall be attributed to its stronger ROS production ability and closer mitochondria interaction. Mitochondria are the power house of cancer cells and a key regulatory center for apoptosis. Western blots analysis also confirmed the upregulation of Cleaved caspase-3 at the expense of Caspase-3 in TPAPyI + L group, proving the occurrence of apoptosis under PDT treatment. (Figure S21). ITPAPyI that specially targets mitochondria and generates ROS directly on mitochondria shall maximize the cell apoptosis rates and therapeutic efficacy.

View Article Online
DOI: 10.1039/D5TB01224D

ARTICLE

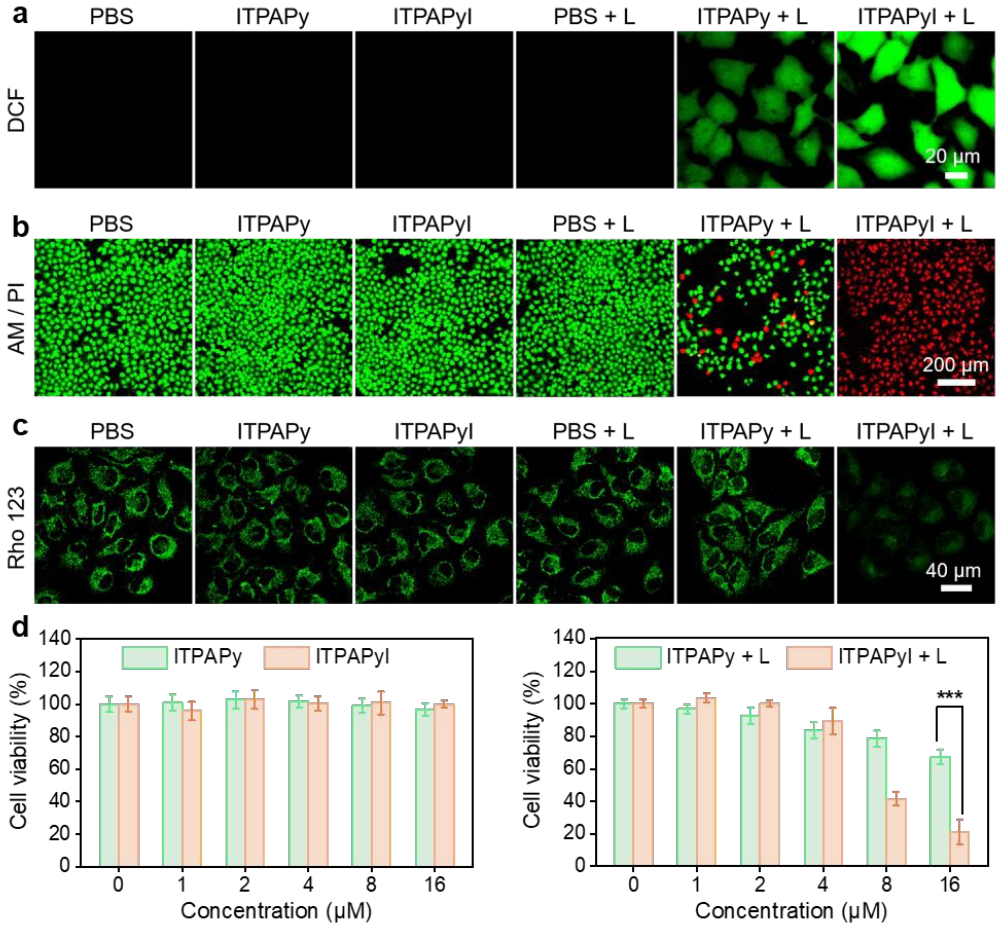

Figure 4. (a) Intracellular ROS detection inside ITPAPy or ITPAPyI treated MCF-7 cells, accessed by DCFH-DA. (b) Live/dead cell staining using calcein-AM (green emission for live cells) and propidium iodide (red emission for dead cells) assays after different treatments. (c) Mitochondrial membrane potential detection inside ITPAPy or ITPAPyI treated MCF-7 cells, accessed by Rho123. (d) Viabilities of MCF-7 cells after treatment by ITPAPy or ITPAPyI with varied concentrations with or without light irradiation. [DCFH-DA] = 20 μM, [Rho123] = 1 μM, [Calcein-AM] = 1 μM,; [PI] = 1 mgmL^{-1}. Data are all presented as the mean ± SD n = 6, *p < 0.05, **p < 0.01, ***p < 0.001.

2.5 *In vivo* PDT of AIE photosensitizers

The PDT performance of the cationic ITPAPyI was further evaluated *in vivo* (Figure 5a). A tumor-bearing mouse was established by inoculating 4T1 cells into the right hind limb site of the mouse. When the tumor volumes reached ~60 mm^3, tumor-bearing mice were randomly divided into four groups (n = 5 mice per group): PBS, PBS + L (L refers to light irradiation), ITPAPyI, and ITPAPyI + L. PBS or ITPAPyI (2 mgmL^{-1}, 100 μL/mouse) were intratumorally injected, and mice in PBS + L and ITPAPyI + L groups were subjected to white light irradiation (200 mWcm^{-1}, 30 min) at 1 h post-injection. The tumor growth and mice weights were consecutively recorded. As shown in Figure 5b, ITPAPyI treatment or light irradiation alone (PBS + L group) exhibited minimal tumor inhibition effect, where the tumors in both groups increased sharply, reaching 10-fold of the initial values, similar to the control PBS group. The cationic photosensitizer ITPAPyI demonstrated remarkable *in vivo* antitumor efficacy when combined with light irradiation, and the tumor volume in the ITPAPyI + L group was reduced to 47% of its initial values. On day 14, the mice were sacrificed and tumors were collected for analysis. Tumors from the ITPAPyI + L group showed the minimal sizes (Figure 5c), and the tumor weights in PBS, PBS + L, ITPAPyI, and ITPAPyI + L groups were further determined to be ~540, ~501, ~402, and ~71 mg (Figure

View Article Online
DOI: 10.1039/D5TB01224D

5d). This pronounced therapeutic effect underscores the critical role of ITPAPyI's tumoricidal activity through mitochondria-targeted photodynamic action.

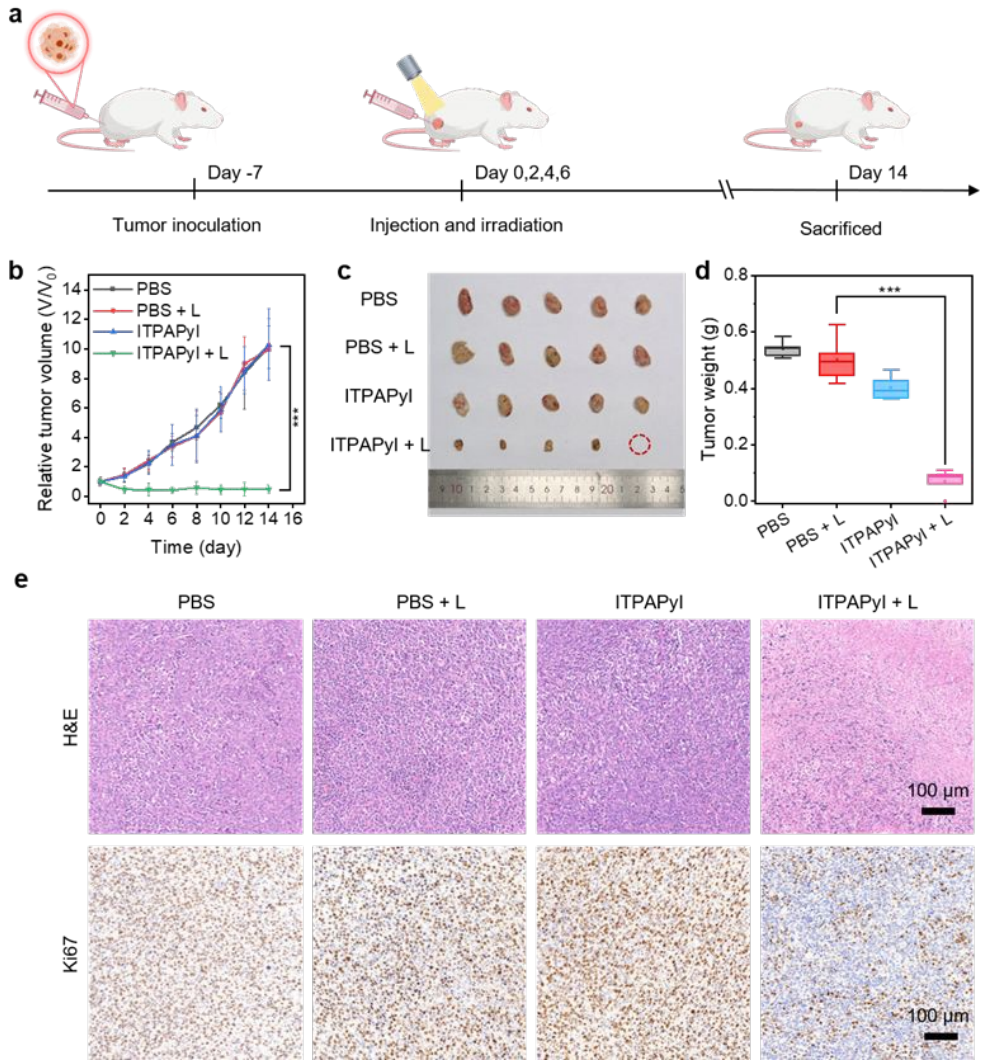

Figure 5. (a) Schematic of the *in vivo* PDT treatment with ITPAPyI. (b)Tumor growth curves in different groups. (c) Photographs of extracted tumors from different groups at day 14. (d) Weights of extracted tumors from different groups. (e) H&E and Ki67 staining images of tumor tissue sections from different groups. Data are all presented as the mean ± SD n = 5, *p < 0.05, **p < 0.01, ***p < 0.001.

View Article Online DOI: 10.1039/D5TB01234D

Tumor tissues were further sliced and stained with hematoxylin and eosin (H&E) and Ki67 to evaluate the therapeutic effects (Figure 5e). The H&E images showed much severe apoptosis and necrosis in the ITPAPyI + L group, which was manifested by extensive chromatin condensation and cell shrinkage. In addition, Ki67-stained images clearly showed that the tumor cells in the ITPAPyI + L group had the lowest proliferative capacity, indicating the excellent tumor ablation ability of ITPAPyI under light irradiation. The biosafety of therapeutic agents in living organisms is a prerequisite for potential biological and clinical applications. No significant difference in the mice body weights in each group throughout the in vivo PDT experiment (Figure S22), H&E staining images of main organs from ITPAPyI + L group showed healthy and similar patterns to the PBS control group (Figure S23), indicating that ITPAPyI was not toxic to mice.

The *in vivo* biocompatibility of ITPAPyI was further evaluated. ITPAPyI was injected into healthy mice via the tail vein with PBS as a controlled benchmark. Blood samples were collected at day 7 post-injection for analysis. As shown in the Figure S24, there were minimal differences in blood routine levels including white blood cell count (WBC), red blood cells (RBC), lymphocytes (Lym#), hematocrit (HCT), mean corpuscular volume (MCV), and hemoglobin (HGB) between ITPAPyI and the control group, indicating that ITPAPyI could not cause infection, anemia, hemorrhage, or other symptoms in healthy mice. In addition, liver and kidney function indexes such as alanine aminotransferase (ALT), aspartate aminotransferase (AST), albumin (ALB), alkaline phosphatase (ALP), urea, creatinine (CREA), and uric acid (UA) were maintained in normal range in the ITPAPyI groups (Figure S25), with minimal difference from the PBS control group. Major organs such as heart, liver, spleen, lungs, and kidneys of mice were also extracted and subjected to H&E staining (Figure S26), which did not show abnormal cell morphology and histopathology, indicating that ITPAPyI does not cause damage to these organisms. Therefore, ITPAPyI demonstrates excellent *in vivo* biocompatibility and biosafety.

3. Conclusion

In summary, we herein report a facile cationization molecular engineering strategy to develop photosensitizers with concurrently enhanced ROS generation and mitochondria targeting ability for PDT. The strategy was demonstrated with AIE photosensitizers ITPAPy and ITPAPyI, which ensure the efficient ROS generation in aggregate state, such as enriching in targeting area. The cationization of the pyridine ring in ITPAPy redistributed the electron distribution, enhanced the ICT effect, facilitating the ISC process and hence triplet formation and ROS generation. As a result, the cationic ITPAPyI showed a 1.24-fold enhanced ROS generation ability. Unlike the neutral AIE photosensitizer ITPAPy which mainly enriched inside lysosome, the cationic ITPAPyI preferably accumulated in cancer cell mitochondria. The improved proximity with mitochondria together with the enhanced ROS generation effectively overcame the short lifespan and small radius of action of ROS, improving the PDT efficacy. The mitochondria membrane damage caused by ITPAPyI was 2.3-fold higher than that caused by ITPAPy under light irradiation. The IC_{50} value was also reduced from 26.91 μM for ITPAPy to 7.08 μM for ITPAPyI. With good biosafety, excellent ROS generation ability, and precise mitochondrial targeting ability, our cationic ITPAPyI exerted a promising antitumor effect in vivo. This study will provide a new approach for the future development of simple and efficient AIE subcellular organelle-targeting photosensitizers for cancer theranostics.

Conflicts of interest

There is no conflict of interest to declare.

Data availability

The data supporting this article have been included as part of the Supplementary Information.

Acknowledgements

This work was financially supported by the National Key R&D Program of China (2024YFA1307601), National Natural Science Foundation of China (22205067, 5247330), Guangdong Provincial Key Laboratory of Luminescence from Molecular Aggregates (2023B1212060003), Guangdong Basic and Applied Basic Research Foundation (2023B1515040003).

Notes and references

1. R. L. Siegel, T. B. Kratzer, A. N. Giaquinto, H. Sung and A. Jemal, *CA-Cancer J. Clin.*, 2025, **75**, 10-45.
2. G. Gunaydin, M. E. Gedik and S. Ayan, *Front. Chem.*, 2021, **9**, 686303.
3. B. Q. Jia, Y. Liu, X. D. Geng, Y. Z. Li, C. M. Zhang, Y. Y. Qu, X. D. Liu, M. W. Zhao, Y. M. Yang, W. F. Li and Y. Q. Li. *Research* 2025, **8**, 0732.
4. Z. Zhou, J. Song, L. Nie and X. Chen, *Chem. Soc. Rev.*, 2016, **45**, 6597-6626.
5. Y. Q. Rao, G. P. Xu, Z. H. Zhang, W. J. Wang, C. M. Zhang, M. W. Zhao, Y. Y. Qu, W. F. Li, M. Ji, Y. G. Liu, and Y. Q. Li, *Chem. Eng. J.*, 2023, **465**, 142961.
6. L. Huang, S. Zhao, J. Wu, L. Yu, N. Singh, K. Yang, M. Lan, P. Wang and J. S. Kim, *Coord. Chem. Rev.*, 2021, **438**, 6597.
7. H. Chen, Y. Wan, X. Cui, S. Li and C. S. Lee, *Adv. Healthcare Mater.*, 2021, **10**, 2101607.
8. J. Li, Z. Zhuang, Z. Zhao and B. Z. Tang, *View*, 2021, **3**, 2.
9. N. Sobhani and A. A. Samadani, *J. Egypt. Natl. Cancer Inst.*, 2021, **33**.
10. G. Li, Q. Wang, J. Liu, M. Wu, H. Ji, Y. Qin, X. Zhou and L. Wu, *J. Mat. Chem. B*, 2021, **9**, 7347-7370.
11. L. Maierhofer, R. Prieto-Montero, T. Cubiella, A. Díaz-Andrés, N. Morales-Benítez, D. Casanova, V. Martínez-Martínez, M.-D. Chiara, E. Mann and J. L. Chiara, *J. Mat. Chem. B*, 2025, **13**, 4330-4340.
12. J. Tian, B. Huang, M. H. Nawaz and W. Zhang, *Coord. Chem. Rev.,*2020, **420**, 213410.

13. D. Xi, N. Xu, X. Xia, C. Shi, X. Li, D. Wang, S. Long, J. Fan, W. Sun and X. Peng, *Adv. Mater.*, 2021, **34**, 2106797.
14. A. Kamkaew, S. H. Lim, H. B. Lee, L. V. Kiew, L. Y. Chung and K. Burgess, *Chem. Soc. Rev.*, 2013, **42**, 77-88.
15. G. Feng, W. Qin, Q. Hu, B. Z. Tang and B. Liu, *Adv. Healthcare Mater.*, 2015, **4**, 2667-2676.
16. J. Sun, Y. Fan, W. Ye, L. Tian, S. Niu, W. Ming, J. Zhao and L. Ren, *Chem. Eng. J.*, 2021, **417**, 128049.
17. Q. Zhan, X. Shi, D. Fan, L. Zhou and S. Wei, *Chem. Eng. J.*, 2021, **404**, 126443.
18. R. Xu, W. Chi, Y. Zhao, Y. Tang, X. Jing, Z. Wang, Y. Zhou, Q. Shen, J. Zhang, Z. Yang, D. Dang and L. Meng, *ACS Nano*, 2022, **16**, 20151-20162.
19. J. Tian, B. Huang, M. H. Nawaz and W. Zhang, *Coord. Chem. Rev.*, 2020, **420**, 213410.
20. M. Chen, Y. Sun and H. Liu, *Interdiscip. Med*. 2023, **1**, e20220012.
21. Z. Li, B. Z. Tang and D. Wang, *Adv. Mater.*, 2024, **36**, 2406047.
22. S. Liu, G. Feng, B. Z. Tang and B. Liu, *Chem. Sci.*, 2021, **12**, 6488-6506.
23. W. Han, S. Zhang, R. Deng, Y. Du, J. Qian, X. Zheng, B. Xu, Z. Xie, F. Yan and W. Tian, *Sci. China Mater.*, 2019, **63**, 136-146.
24. F. Sun, Y. Chen, K. W. K. Lam, W. Du, Q. Liu, F. Han, D. Li, J. W. Y. Lam, J. Sun, R. T. K. Kwok and B. Z. Tang, *Small*, 2024, **20**, 202401334.
25. Z. Zhu, Y. Shi, C. Yan, M. Liu, W.-H. Zhu and Z. Su, *Coord. Chem. Rev.*, 2025, **533**, 216550.
26. H. Wang, E. Zhao, J. W. Y. Lam and B. Z. Tang, *Mater. Today*, 2015, **18**, 365-377.
27. Z. Zhuang, J. Li, P. Shen, Z. Zhao and B. Z. Tang, *Aggregate*, 2024, **5**, e540.
28. J. Gao, Y. Tian, Y. Li, F. Hu and W. Wu, *Coord. Chem. Rev.*, 2024, **507**, 215756.
29. Z. Liu, Z. Tang, Y. Yin, M. Wan, J. Zhan and L. Ren, *Adv. Healthcare Mater.*, 2025, **14**, 2403954.
30. T. Zhang, X. Yang, X. Ou, M. M. S. Lee, J. Zhang, C. Xu, X. Yu, P. Gong, J. W. Y. Lam, P. Zhang and B. Z. Tang, *Adv. Mater.*, 2023, **35**, 2303186.
31. K. Ni, G. Lan, S. S. Veroneau, X. Duan, Y. Song and W. Lin, *Nat. Commun.*, 2018, **9**, 4321.
32. S. Xie, C. Liu, Y. Cao, J. Xia and B. Lu, *Sci. China Mater.*, 2025, **68**, 1285-1291.
33. A. H. Mehmood, F. Ullah, B. Dong and H. Liu, *Sci. China Mater.*, 2024, **67**, 3491-3530.
34. X. Guo, N. Yang, W. Ji, H. Zhang, X. Dong, Z. Zhou, L. Li, H. M. Shen, S. Q. Yao and W. Huang, *Adv. Mater.*, 2021, **33**, 2007778.
35. J. Liu, X. Liu, M. Wu, G. Qi and B. Liu, *Nano Lett.*, 2020, **20**, 7438-7445.
36. N. Kiweler, C. Delbrouck, V. I. Pozdeev, L. Neises, L. Soriano-Baguet, K. Eiden, F. Xian, M. Benzarti, L. Haase, E. Koncina, M. Schmoetten, C. Jaeger, M. Z. Noman, A. Vazquez, B. Janji, G. Dittmar, D. Brenner, E. Letellier and J. Meiser, *Nat. Commun.*, 2022, **13**, 2699.
37. E. R. H. Walter, P. K.-K. Leung, L. C.-C. Lee, K. K.-W. Lo and N. J. Long, *J. Mater. Chem. B*, 2024, **12**, 10409-10415.
38. W. Lv, Z. Zhang, K. Y. Zhang, H. Yang, S. Liu, A. Xu, S. Guo, Q. Zhao and W. Huang, *Angew. Chem. Int. Ed.*, 2016, **55**, 9947-9951.
39. F. Tong, Y. Wang, Y. Xu, Y. Zhou, S. He, Y. Du, W. Yang, T. Lei, Y. Song, T. Gong and H. Gao, *Nat. Commun.*, 2024, **15**.
40. H. Zhang, C. Wang, K. Wang, X. Xuan, Q. Lv and K. Jiang, *Biosens. Bioelectron.*, 2016, **85**, 96-102.
41. H. Singh, D. Sareen, J. M. George, V. Bhardwaj, S. Rha, S. J. Lee, S. Sharma, A. Sharma and J. S. Kim, *Coord. Chem. Rev.*, 2022, **452**, 214283.
42. D. Li, E. Ha, Y. Zhu, S. He, S. Kuang and J. Hu, *Sci. China Mater.*, 2025, **68**, 1648-1657.
43. Y. Peng, R. Mo, M. Yang, H. Xie, F. Ma, Z. Ding, S. Wu, J. W. Y. Lam, J. Du, J. Zhang, Z. Zhao and B. Z. Tang, *ACS Nano*, 2024, **18**, 26140−26152
44. L. Ren, P. Xu, J. Yao, Z. Wang, K. Shi, W. Han and H. Wang, *ACS Nano*, 2022, **16**, 10242-10259.
45. D. Shang, Q. Yu, W. Liu, S. Zhang, Y. Li, J. Chen, Z. Zhang and X. Lu, *Sci. China Mater.*, 2021, **65**, 527-535.
46. Z. Liu, H. Zou, Z. Zhao, P. Zhang, G.-G. Shan, R. T. K. Kwok, J. W. Y. Lam, L. Zheng and B. Z. Tang, *ACS Nano*, 2019, **13**, 11283-11293.
47. Y. Yu, S. Wu, L. Zhang, S. Xu, C. Dai, S. Gan, G. Xie, G. Feng and B. Z. Tang, *Biomaterials*, 2022, **280**, 121255
48. S. Liu, B. Wang, Y. Yu, Y. Liu, Z. Zhuang, Z. Zhao, G. Feng, A. Qin and B. Z. Tang, *ACS Nano*, 2022, **16**, 9130-9141.
49. T. Zhao, Y. Xu, R. Liu, X. Shang, C. Huang, W. Dong, M. Long, B. Zou, X. Wang, G. Li, Y. Shen, T. Liu and B. Tang, *Adv. Healthcare Mater.*, 2023, **12**, 2301035.
50. T. C. Pham, V.-N. Nguyen, Y. Choi, S. Lee and J. Yoon, *Chem. Rev.*, 2021, **121**, 13454-13619.
51. H. Qi, S. Wang, Z. Gao, D. Xie, J. Li, Y. Liu, S. Xue, S. Ying, D. Ma and S. Yan, *ACS Materials Lett.*, 2024, **6**, 3844-3853.
52. Y. Bu, T. Xu, X. Zhu, J. Zhang, L. Wang, Z. Yu, J. Yu, A. Wang, Y. Tian, H. Zhou and Y. Xie, *Chem. Sci.*, 2020, **11**, 10279-10286.
53. S. Chen, X. Liu, X. Ge, Q. Wang, Y. Xie, Y. Hao, Y. Zhang, L. Zhang, W. Shang and Z. Liu,Inorg. *Chem. Front.*, 2020, **7**, 91-100.
54. Q. Xiao, H. Lin, J. Wu, X. Pang, Q. Zhou, Y. Jiang, P. Wang, W. Leung, H. Lee, S. Jiang, S. Q. Yao, L. Gao, G. Liu and C. Xu, *J. Med. Chem.*, 2020, **63**, 4896-4907.
55. K. Wang, Y. Liu, C. Liu, H. Zhu, X. Li, F. Zhang, N. Gao, X. Pang, W. Sheng and B. Zhu, *New J. Chem.*, 2021, **45**, 14548-14553.
56. H. T. Xin, Q. W. Lin, S. Sun, Y. Y. Wang, B. Liu, W. J. Wang, Z. W. Mao and K. N. Wang, *Aggregate*, 2024, **6**, e709.

View Article Online
DOI: 10.1039/D5TB01224D

Data availability statement

The data supporting this article have been included as part of the Supplementary Information.